Rapid Communications

Perovskite $ThTaN_3$: A large-thermopower topological crystalline insulator

Myung-Chul Jung,[1] Kwan-Woo Lee,[1,2,*] and Warren E. Pickett[3,†]
[1]*Department of Applied Physics, Graduate School, Korea University, Sejong 30019, Korea*
[2]*Division of Display and Semiconductor Physics, Korea University, Sejong 30019, Korea*
[3]*Department of Physics, University of California, Davis, California 95616, USA*

(Received 4 September 2017; published 8 March 2018)

$ThTaN_3$, a rare cubic perovskite nitride semiconductor, has been studied using *ab initio* methods. Spin-orbit coupling (SOC) results in band inversion and a band gap of 150 meV at the zone center. Despite trivial Z_2 indices, two pairs of spin-polarized surface bands cross the gap near the zone center, indicating that this system is a topological crystalline insulator with the mirror Chern number of $|\mathcal{C}_m| = 2$ protected by the mirror and C_4 rotational symmetries. Additionally, SOC doubles the Seebeck coefficient, leading to a maximum of $\sim$400 μV/K at 150 K for carrier-doping levels of several $10^{17}/\text{cm}^3$. $ThTaN_3$ combines excellent bulk thermopower with parallel conduction through topological surface states that may point toward new possibilities for platforms for engineering devices with larger figures of merit.

DOI: 10.1103/PhysRevB.97.121104

I. INTRODUCTION

After the discovery of time-reversal Z_2 topological insulators (TIs) [1], Fu proposed another type of TI protected by crystal symmetries, such as mirror or rotational symmetry [2]. This class is called the topological crystalline insulator (TCI), expected to display exotic quantum phenomena including topological superconductivity [3]. Through model calculations in three-dimensional systems, Fu suggested both the n-fold rotation C_n ($n = 4,6$) and the time-reversal symmetries [2] could produce the TCI, whereas Alexandradinata *et al.* [4] and Alexandradinata and Bernevig [5] further proposed that n-fold rotation and reflection C_{nv} symmetries of $n = 3$, 4, and 6 may lead to the TCI without help of the time-reversal symmetry. In contrast to ordinary TIs, need for spin-orbit coupling (SOC) is not a requirement for a TCI, but many prospective TCI materials suggested by first-principles calculations require SOC to invert band characters as in $ThTaN_3$ investigated here. However, SOC will affect the final gap size, so heavy atoms may still be more favorable as in conventional TIs.

The combination of large bulk thermopower and gapless TI boundary states represents a new frontier in topological materials. In finite samples the conductivity provided by (topological) surface states impacts the resulting thermopower as discussed by two groups [6,7]. The surface conductance leads to an anomalous Seebeck effect that can be tuned by engineering the size and shape of the sample. The first TCIs were proposed in IV-VI semiconductors of a simple rock-salt structure with mirror symmetry [8,9], such as SnTe, PbTe, PbSe, SnS, and SnSe, which had been known as good thermoelectric materials [10,11]. Soon after these theoretical predictions, the topological character of these compounds was observed [12–14], specifically, a double Dirac-cone structure through (spin) angle-resolved photoemission spectroscopy (ARPES).

In contrast to the ordinary Z_2 index class of TIs showing an odd number of Dirac points in a surface state, TCIs have an even number of Dirac points [8]. Moreover, scanning tunneling microscopy and ARPES studies showed massive Dirac cones induced by breaking the symmetry in these TCIs, suggesting a possibility for engineering the Dirac band gap [15–17]. Their two-dimensional monolayer cousins are also suggested to support TCI phases [18,19]. It has been suggested that the rock-salt structure PbPo shows both TCI and ferroelectric instability [20]. In addition to the rock-salt compounds, TCI phases have been theoretically predicted in pyrochlore oxides [21], antiperovskite compounds [22], the orthorhombic perovskite $SrIrO_3$ [23], and full-Heusler compounds [24]. However, exotic physical properties of TCIs have not been established due to the lack of the combination of both theoretical predictions and experimental realization.

In this Rapid Communication we investigate topological and thermoelectric properties of the time-reversal symmetric cubic perovskite nitride $ThTaN_3$ possessing both the fourfold rotation and the mirror symmetries utilized by Fu [2] but now using first-principles approaches. Nitride perovskites are quite rare compared to the oxides [26] and with different properties, including that itinerant hole or electron doping is expected to be much easier in the nitride [27] due to the smaller electronegativity and larger polarizability of N relative to O. The cubic perovskite insulator $ThTaN_3$, displayed in Fig. 1(a), was obtained using solid-state synthesis methods by Brese and DiSalvo [28], but characterization has been limited. Theoretical calculations have confirmed the semiconducting character and stability of the cubic phase [29–31]. The results we present indicate that perovskite $ThTaN_3$ is not only a TCI, but also displays highly favorable thermoelectric properties.

The organization of this Rapid Communication is as follows. The theoretical methods are presented in Sec. II. Section III contains the main results on the electronic structure, the TCI characteristics, and the carrier density and temperature dependence of the thermopower. In Sec. IV we provide a brief summary.

*mckwan@korea.ac.kr
†pickett@physics.ucdavis.edu

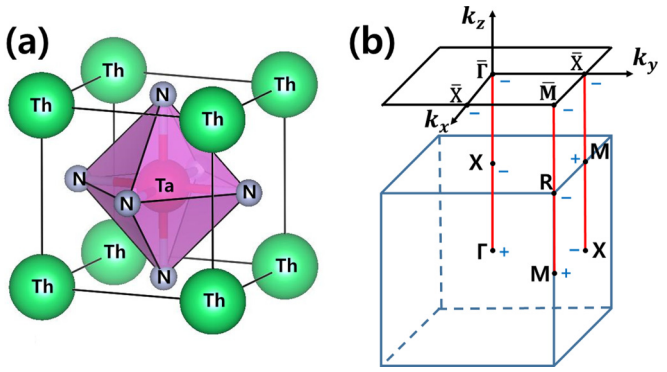

FIG. 1. (a) Crystal structure of $ThTaN_3$, plotting using the VESTA program [25]. (b) Bulk and (001) surface Brillouin zones (BZs) with high-symmetry points. The ± symbols represent the party of all occupied bands of $ThTaN_3$ at each time-reversal invariant momentum (TRIM).

II. THEORETICAL APPROACH

The experimental diffraction data [28] indicate the cubic perovskite structure, and density functional calculations obtain positive elastic constants for the cubic structure [29]. Our *ab initio* calculations, performed using the experimental lattice parameter $a = 4.02$ Å [28] which is close to our optimized value of 4.06 Å, were performed using the accurate all-electron full-potential code WIEN2K. [32]. Selected results were confirmed with another all-electron full-potential code FPLO [33]. The Perdew-Burke-Ernzerhof generalized gradient approximation (GGA) was used as the exchange-correlation functional [34]. SOC has been included in the results we present except where noted. The Brillouin zone was sampled with a uniform fine k mesh of $21 \times 21 \times 21$ to check the narrow gap nature carefully. In WIEN2K, the basis was determined by $R_{\rm mt}K_{\rm max} = 7$ and augmented atomic radii in atomic units: Th 2.4, Ta 2.0, and N 1.7. For FPLO the default basis functions for the constituent atoms were used. The second variation procedure [35] is used to include SOC effects in WIEN2K. About 1-Ry width of conduction bands is kept for the second diagonalization, giving nearly perfect convergence of the SOC calculation.

To investigate for topological character, our calculated band structure and eigenfunctions were fit using the WANNIER90 code [36] with an initial basis of N $2p$, Ta $5d$, Th $6d$, and $5f$ orbitals, resulting in an excellent fit in the range of -7 to 4 eV relative to the Fermi level E_F [see Fig. 2(a)]. From these results, the surface states were calculated through the Green's-function approach implemented in the WANNIERTOOLS code [37]. The hybrid Wannier charge center is also provided by the Z2PACK code [38].

Thermoelectric properties were studied using the BOLTZTRAP code [39] based on the semiclassical Bloch-Boltzmann transport theory [40] with a constant scattering time approximation. The applicability of this approach and the accuracy of the BOLTZTRAP code in similar systems has been well established [10,41,42]. A much denser regular k mesh containing up to 60 000 k points was used since these calculations were very sensitive to the details of the band structure in the region of the gap.

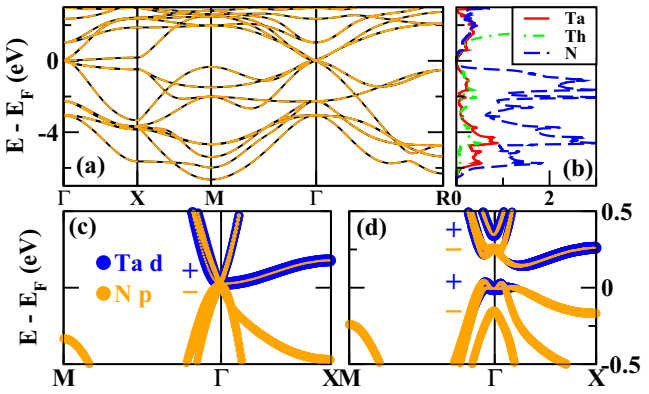

FIG. 2. Top: (a) Nonmagnetic GGA band structure of $ThTaN_3$ in the region containing N $2p$, Ta $5d$, and Th $6d$ and $5f$ orbitals. The nearly flat Th $5f$ bands appear around 3 eV, relative to the Fermi level E_F which is set to zero. The orange dashed lines indicate bands obtained from Wannier interpolation, showing an excellent representation of the bands. (b) The corresponding atom-projected densities of states (DOSs) in units of states per eV. Bottom: enlarged fatband structures of (c) GGA and (d) GGA + SOC along the M-Γ-X line near E_F. The band inversion induced by SOC at the Γ point is evident in panel (d). With SOC included, at the Γ point the characters of each band are the singlet N p, doublet Ta d, doublet N p, and singlet Ta d from the lower to the higher energies. The ± symbols at the Γ point denote the parity of each band.

III. RESULTS

A. Electronic structure

First we address the electronic structure obtained with a dense k mesh to investigate the character of its small gap carefully. The full range GGA band structure and the corresponding atom-resolved DOSs given in Figs. 2(a) and 2(b), respectively, indicate that this system is a small gap band insulator [43], consistent with the formal charge configuration of Ta^{5+}, Th^{4+}, and N^{3-}. The valence bands have the fully filled N $2p$ character, whereas the bottom of the conduction bands has the Th t_{2g} character as shown in Figs. 2(c) and 2(d). Thus $ThTaN_3$ shows a common p-d direct gap between two threefold degenerate bands at the zone center.

Now specific effects of SOC are considered. The bottom panels of Fig. 2 show enlarged band structures of GGA and GGA + SOC overlapped by the fatband coloring showing Ta $5d$ and N $2p$ characters. Inclusion of SOC leads to splitting the threefold bands on either side of the gap into a doublet and singlet and enhancing the energy gap to 150 meV. The gap is smaller by 10 meV at the optimized volume. Most importantly, the band splitting results in band inversion at Γ. As shown in Fig. 2(c), before SOC the threefold band at the top of the valence band arising from $2p$ states of all N ions has negative parity, whereas the Ta t_{2g} triplet at the bottom of the conduction band has positive parity. SOC results in splitting and inverting the parities: The parity of each band in the doublet at the bottom of the conduction band is negative [see Fig. 2(d)]. This band inversion suggests a nontrivial topological character as will be discussed in the next subsection.

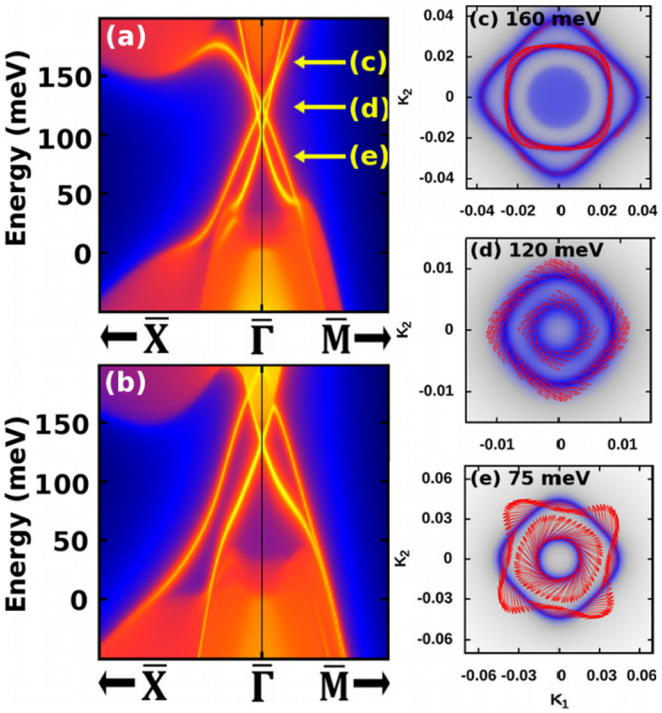

FIG. 3. The (001) surface spectral functions (SOC included) obtained from the Green's-function method for (a) ThN and (b) TaN_2 terminations. The Fermi contours are shown in blue. Without SOC (not shown here), no surface band appears. Panels (c)–(e) display the spin texture (shown with the red arrows), having only in-plane components on the double Dirac cone at energies denoted in panel (a). The arrows provide the spin direction. Note the changes in scale in panels (c)–(e).

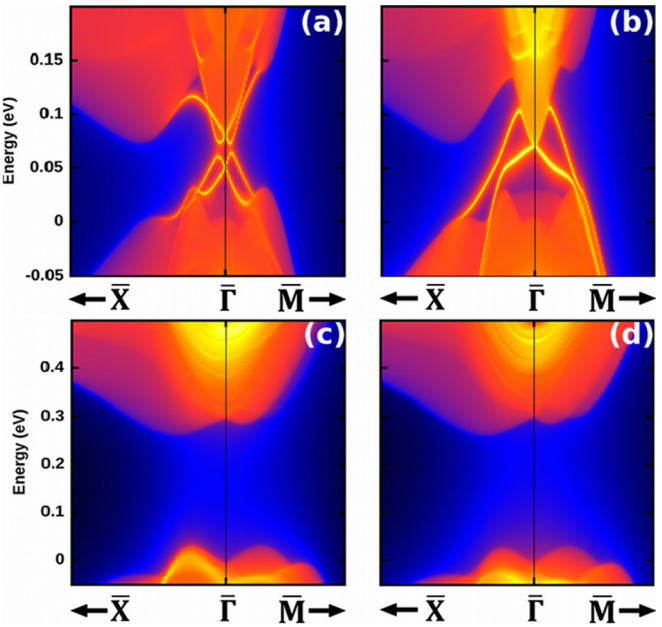

FIG. 4. The (001) surface spectral function (SOC included) of ThN (left) and TaN_2 (right) terminations when breaking symmetries. For the upper panel, the Ta ion is displaced by 0.01 Å in the (100) direction to remove only the mirror symmetry. For the low panel, the ion is displaced by the same amount in the (111) direction to break both the mirror and the rotational symmetries.

B. Topological crystalline insulating phase

Our calculations of the topological character begin from the Wannier representation [36], shown in Fig. 2(a). The Z_2 indices $\nu_0;(\nu_1\nu_2\nu_3)$ are calculated [44] from the parties of all occupied bands, excluding the core orbitals, at TRIMs, shown in Fig. 1(b). The indices are 0;(000), indicating that $ThTaN_3$ is topologically trivial. Specifically, two negative-parity valence-band states have interchanged with two positive-parity conduction-band states, and the change in occupied TRIM parities by two leaves vanishing Z_2 indices. To gather further evidence, the hybrid Wannier charge centers are calculated for half of the BZ on the mirror plane [38]. Consistent with the Z_2 indices, the hybrid center plot shows an even number of crossings, indicating that a Z_2 TI has not emerged (see the Supplemental Material [45]).

Next, we performed surface-state calculations by the Green's-function approach. Figures 3(a) and 3(b) show the surface spectral functions for ThN and TaN_2 surface terminations, respectively, using (001) surfaces [given the cubic symmetry, only (001) needs to be considered]. For both terminations, two pairs of surface bands crossing the gap appear at the zone center, although distinctions verify that they are inequivalent.

The spin textures, pictured in Figs. 3(c)–3(e), are calculated in three regimes: below the lower Dirac point, above the upper Dirac point, and midway between the two points. At 160 meV in Fig. 3(c), the texture on the outer Fermi contour is clockwise with opposite chirality on the inner contour. At 120 meV [the intermediate regime, Fig. 3(d)] both textures are counterclockwise. At 75 meV the texture on the outer Fermi contour is counterclockwise with opposite chirality on the inner contour.

To reveal the origin of this topological character, crystalline symmetries have been broken by displacing the Ta ion in two directions [45]. First, the ion was displaced by 0.01 Å along the (100) direction to remove the $x \to -x$ mirror symmetry. The upper panel of Fig. 4 shows that elimination of this mirror symmetry destroys the surface state of the ThN termination (the disconnect of bands near 0.06 eV energy), whereas that of TaN_2 survives. Second, both the mirror and the rotational symmetries were discarded by shifting Ta along the (111) direction by 0.01 Å. The bottom panel of Fig. 4 reveals that both surface states have disappeared. This killing of surface bands by breaking of symmetry is evidence that $ThTaN_3$ is a TCI protected by C_4 symmetry rather than by mirror symmetry. Similar effects have been observed in the antiperovskite compounds [22]. Also, these two pairs of surface bands indicate that the mirror Chern number $\mathcal{C}_M = (\mathcal{C}_{+i} - \mathcal{C}_{-i})/2$ is two, where $\mathcal{C}_{\pm i}$'s are individual Chern numbers for Bloch eigenstates with eigenvalues $\eta = \pm i$ [46]. Note that two Dirac cones in $ThTaN_3$ concurrently emerge at $\bar{\Gamma}$, in contrast to the previous TCIs with $|\mathcal{C}_M| = 2$ [8,19], which have two Dirac cones separately appearing at two different TRIMs.

C. Thermoelectric properties

As mentioned above, the first TCIs were realized in promising thermoelectric compounds [8,9]. There is however no di-

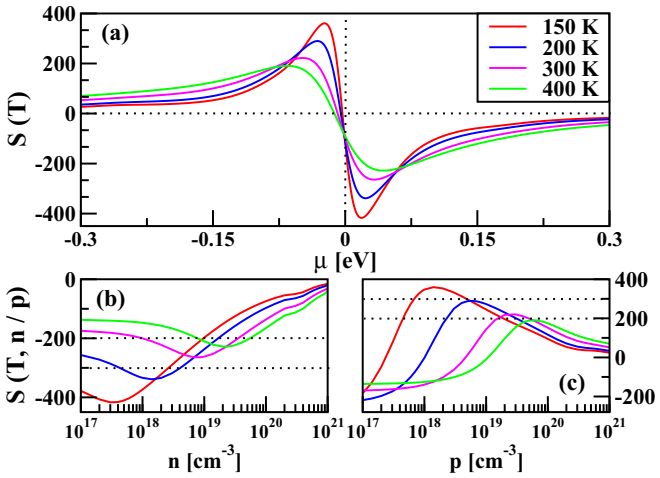

FIG. 5. Seebeck coefficients $S(T)$ (in units of μV/K) versus (a) band filling μ, (b) and (c) concentration of doped carriers at various temperatures in the range of 150–400 K; SOC is included. This behavior is similar to that without SOC (not shown here) but is roughly doubled by SOC.

rect relation between thermoelectric and topological properties aside from the commonality of possessing small band gaps. First, thermoelectric properties are a bulk property, whereas the impact of the topological character resides in the boundary states. The Seebeck coefficient is determined solely by the bands $E(\vec{k})$, their derivatives, and the Fermi level E_F [40], whereas the topological states are the result of topological features arising from inversion and mixing of the bulk valence and conduction bands. Nevertheless, one may simplistically anticipate that a high thermopower is achieved in TCIs or TIs with a narrow gap since SOC, which is often significant in topological matters, leads to considerable changing in dispersion around E_F, hence may provide the steep DOS that often signals large thermopower. Such a connection occurs in this system as we now discuss.

As shown in Figs. 2(b) and 2(c), inclusion of SOC substantially reduces the dispersion of the doubly degenerate bands at the top of the valence band and the bottom of the conduction band along the Γ-X line, resulting in a steeper DOS that roughly doubles the Seebeck coefficient. Figure 5 shows $S(T)$ (SOC included) over the range of 150–400 K in temperature. Due to the narrow gap, $S(T)$ rapidly increases in magnitude at very small levels of doping and reaches the very large value of $\sim$400 μV/K at 150 K. Upon increasing T, the maximum in $S(T)$ monotonically decreases. However, it retains excellent thermoelectric performance (200–300 μV/K) [47], indicated by the dashed lines in Fig. 5, over a range of 10^{17}/cm^{-3}–10^{19}/cm^{-3} doping level (i.e., $\sim 10^{-4}$–10^{-6} carriers per formula unit) below $T = 400$ K.

IV. SUMMARY

In $ThTaN_3$, which is a rare cubic nitride perovskite, spin-orbit coupling leads to enlarging the gap to 150 meV and inverting valence and conduction bands. Interestingly, two surface band Dirac cones in the gap concurrently appear at the zone center, although this system shows trivial Z_2 indices and character of the hybrid Wannier charge center. This even number of surface bands indicates that $ThTaN_3$ is a topological crystalline insulator with the mirror Chern number $|\mathcal{C}_m| = 2$, protected by the mirror and fourfold rotational symmetries. Additionally, due to the narrow gap and less dispersive bands near E_F induced by SOC, this system shows a very high Seebeck coefficient with a maximum of $\sim$400 μV/K at 150 K, suggesting a possible application as an element in a thermoelectric device (see the Supplemental Material [45]).

Our findings indicate that stoichiometric $ThTaN_3$ is a TCI also with good thermoelectric properties, inviting further theoretical and experimental research. Most currently known topological insulators suffer from defects in the bulk that degrade the insulating bulk to semiconducting, thus precluding identification of and therefore application of the topological surface bands. The sample quality did not allow determination of stoichiometry in $ThTaN_3$ [28], but this material is chemically distinct from previous TIs and thus provides new opportunities.

ACKNOWLEDGMENTS

We acknowledge Y.-K. Kim for a useful discussion of topological insulators and K.-H. Ahn and Y.-J. Song for useful technical discussions. Discussions on nitride perovskites with A. P. Ramirez, M. Subramanian, and T. Siegrist were appreciated. This research was supported by NRF of Korea Grant No. NRF-2016R1A2B4009579 (M.C.J. and K.W.L) and by U.S. DOE BES Grant No. DE-FG02-04ER46111 (W.E.P.).

[1] C. L. Kane and E. J. Mele, Quantum Spin Hall Effect in Graphene, Phys. Rev. Lett. **95**, 226801 (2005).

[2] L. Fu, Topological Crystalline Insulators, Phys. Rev. Lett. **106**, 106802 (2011).

[3] For a review, see Y. Ando and L. Fu, Topological crystalline insulators and topological superconductors: From concepts to materials, Annu. Rev. Condens. Matter Phys. **6**, 361 (2015).

[4] A. Alexandradinata, C. Fang, M. J. Gilbert, and B. A. Bernevig, Spin-Orbit-Free Topological Insulators without Time-Reversal Symmetry, Phys. Rev. Lett. **113**, 116403 (2014).

[5] A. Alexandradinata and B. A. Bernevig, Berry-phase description of topological crystalline insulators, Phys. Rev. B **93**, 205104 (2016).

[6] Y. Xu, Z. Gan, and S. C. Zhang, Enhanced Thermoelectric Performance and Anomalous Seebeck Effects in Topological Insulators, Phys. Rev. Lett. **112**, 226801 (2014).

[7] For a review, see N. Xu, Y. Xu, and J. Zhu, Topological insulators for thermoelectrics, npj Quantum Mater. **2**, 51 (2017).

[8] T. H. Hsieh, H. Lin, J. Liu, W. Duan, A. Bansil, and L. Fu, Topological crystalline insulators in the SnTe material class, Nat. Commun. **3**, 982 (2012).

[9] Y. Sun, Z. Zhong, T. Shirakawa, C. Franchini, D. Li, Y. Li, S. Yunoki, and X.-Q. Chen, Rocksalt SnS and SnSe: Native topological crystalline insulators, Phys. Rev. B **88**, 235122 (2013).

[10] D. J. Singh, Doping-dependent thermopower of PbTe from Boltzmann transport calculations, Phys. Rev. B **81**, 195217 (2010).

[11] S. Roychowdhury, U. S. Shenoy, U. V. Waghmare, and K. Biswas, Tailoring of electronic structure and thermoelectric properties of a topological crystalline insulator by chemical doping, Angew. Chem. Int. Ed. **54**, 15241 (2015).

[12] Y. Tanaka, Z. Ren, T. Sato, K. Nakayama, S. Souma, T. Takahashi, K. Segawa, and Y. Ando, Experimental realization of a topological crystalline insulator in SnTe, Nat. Phys. **8**, 800 (2012).

[13] P. Dziawa, B. J. Kowalski, K. Dybko, R. Buczko, A. Szczerbakow, M. Szot, E. Łusakowska, T. Balasubramanian, B. M. Wojek, M. H. Berntsen, O. Tjernberg, and T. Story, Topological crystalline insulator states in $Pb_{1-x}Sn_xSe$, Nature Mater. **11**, 1023 (2012).

[14] S.-Y. Xu, C. Liu, N. Alidoust, M. Neupane, D. Qian, I. Belopolski, J. D. Denlinger, Y. J. Wang, H. Lin, L. A. Wray, G. Landolt, B. Slomski, J. H. Dil, A. Marcinkova, E. Morosan, Q. Gibson, R. Sankar, F. C. Chou, R. J. Cava, A. Bansil, and M. Z. Hasan, Observation of a topological crystalline insulator phase and topological phase transition in $Pb_{1-x}Sn_xTe$, Nat. Commun. **3**, 1192 (2012).

[15] Y. Okada, M. Serbyn, H. Lin, D. Walkup, W. Zhou, C. Dhital, M. Neupane, S. Xu, Y. J. Wang, R. Sankar, F. Chou, A. Bansil, M. Z. Hasan, S. D. Wilson, L. Fu, and V. Madhavan, Observation of dirac node formation and mass acquisition in a topological crystalline insulator, Science **341**, 1496 (2013).

[16] I. Zeljkovic, Y. Okada, M. Serbyn, R. Sankar, D. Walkup, W. Zhou, J. Liu, G. Chang, Y. J. Wang, M. Z. Hasan, F. Chou, H. Lin, A. Bansil, L. Fu, and V. Madhavan, Dirac mass generation from crystal symmetry breaking on the surfaces of topological crystalline insulators, Nature Mater. **14**, 318 (2015).

[17] B. M. Wojek, M. H. Bernsten, V. Jonsson, A. Szczerbakow, P. Dziawa, B. J. Kowalski, T. Story, and O. Tjernberg, Direct observation and temperature control of the surface Dirac gap in a topological crystalline insulator, Nat. Commun. **6**, 8463 (2015).

[18] E. O. Wrasse and T. M. Schmidt, Prediction of Two-Dimensional Topological Crystalline Insulator in PbSe Monolayer, Nano Lett. **14**, 5717 (2014).

[19] J. Liu, X. Qian, and L. Fu, Crystal field effect induced topological crystalline insulators in monolayer IV-VI semiconductors, Nano Lett. **15**, 2657 (2015).

[20] C.-J. Kang and B. I. Min, Ferroelectric instability and topological crystalline insulating nature in PbPo, Phys. Rev. B **93**, 041104(R) (2016).

[21] M. Kargarian and G. A. Fiete, Topological Crystalline Insulators in Transition Metal Oxides, Phys. Rev. Lett. **110**, 156403 (2013).

[22] T. H. Hsieh, J. Liu, and L. Fu, Topological crystalline insulators and Dirac octets in antiperovskites, Phys. Rev. B **90**, 081112(R) (2014).

[23] Y. Chen, Y.-M. Lu, and H.-Y. Kee, Topological crystalline metal in orthorhombic perovskite iridates, Nat. Commun. **6**, 6593 (2015).

[24] A. Pham and S. Li, Unique topological surface states of full-Heusler topological crystalline insulators, Phys. Rev. B **95**, 115124 (2017).

[25] K. Momma and F. Izumi, VESTA: A three-dimensional visualization system for electronic and structural analysis, J. Appl. Crystallogr. **41**, 653 (2008).

[26] R. Sarmiento-Pérez, T. F. T. Cerqueira, S. Körbel, S. Botti, and M. A. L. Marques, Prediction of stable nitride perovskites, Chem. Mater. **27**, 5957 (2015).

[27] A. S. Botana, V. Pardo, and W. E. Pickett, All 3*d* Electron-Hole Bilayers in CrN/MgO(111) Multilayers for Thermoelectric Applications, Phys. Rev. Appl. **7**, 024002 (2017).

[28] N. E. Brese and F. J. DiSalvo, Synthesis of the first thorium-containing nitride perovskite $TaThN_3$, J. Solid State Chem. **120**, 378 (1995).

[29] V. V. Bannikov, I. R. Shein, and A. L. Ivanovskii, Electronic structure, chemical bonding, and elastic properties of the first thorium-containing nitride perovskite $TaThN_3$, Phys. Status Solidi RRL **1**, 89 (2007).

[30] S. F. Matar and G. Demazeau, Potential existence of post-perovskite nitrides: DFT studies of $ThTaN_3$, J. Solid State Chem. **183**, 994 (2010).

[31] J. M. Polfus and R. Haugsrud, Protons in perovskite nitrides and oxide nitrides: A first principles study of $ThTaN_3$ and $SrTaO_2N$, Solid State Commun. **152**, 1921 (2012).

[32] K. Schwarz and P. Blaha, Solid state calculations using WIEN2k, Comput. Mater. Sci. **28**, 259 (2003).

[33] K. Koepernik and H. Eschrig, Full-potential nonorthogonal local-orbital minimum-basis band-structure scheme, Phys. Rev. B **59**, 1743 (1999).

[34] J. P. Perdew, K. Burke, and M. Ernzerhof, Generalized Gradient Approximation Made Simple, Phys. Rev. Lett. **77**, 3865 (1996).

[35] A. H. MacDonald, W. E. Pickett, and D. D. Koelling, A linearized relativistic augmented plane-wave method utilizing approximate pure-spin basis functions, J. Phys. C **13**, 2675 (1980).

[36] A. A. Mostofi, J. R. Yates, G. Pizzi, Y. Lee, I. Souza, D. Vanderbilt, and N. Marzari, An updated version of wannier90: A tool for obtaining maximally-localized Wannier functions, Comput. Phys. Commun. **185**, 2309 (2014).

[37] Q. S. Wu, S. N. Zhang, H.-F. Song, M. Troyer, and A. A. Soluyanov, WannierTools: An open-source software package for novel topological materials, Comput. Phys. Commun. **224**, 405 (2018).

[38] A. A. Soluyanov and D. Vanderbilt, Computing topological invariants without inversion symmetry, Phys. Rev. B **83**, 235401 (2011); D. Gresch, G. Autés, O. V. Yazyev, M. Troyer, D. Vanderbilt, B. Andrei Bernevig, and A. A. Soluyanov, Z2Pack: Numerical implementation of hybrid Wannier centers for identifying topological materials, *ibid.* **95**, 075146 (2017).

[39] G. K. H. Madsen and D. J. Singh, BoltzTraP. A code for calculating band-structure dependent quantities, Comput. Phys. Commun. **175**, 67 (2006).

[40] P. B. Allen, W. E. Pickett, and H. Krakauer, Anisotropic normal-state transport properties predicted and analyzed for high-T_c oxide superconductors, Phys. Rev. B **37**, 7482 (1988).

[41] A. Dewandre, O. Hellman, S. Bhattacharya, A. H. Romero, G. K. H. Madsen, and M. J. Verstraete, Two-Step Phase

Transition in SnSe and the Origins of its High Power Factor from First Principles, Phys. Rev. Lett. **117**, 276601 (2016).

[42] J. Zhang, L. Song, S. H. Pedersen, H. Yin, L. T. Hung, and B. B. Iversen, Discovery of high-performance low-cost n-type Mg_3Sb_2-based thermoelectric materials with multi-valley conduction bands, Nat. Commun. **8**, 13901 (2017).

[43] Using three different codes WIEN2K, FPLO, and VASP, [48] our careful calculations with a dense k mesh indicate that $ThTaN_3$ is either metallic or insulating with a tiny gap of several meV within the GGA, differences that are typical between different codes. Our value of the gap is different from the previous reports in Refs. [29], [30], [31] online which quote energy gaps of 0.4–0.8 eV. However, one of them included an artificial factor to enhance the gap [29]. The largest value was also obtained with a hybrid functional [31]. Thus the main difference in the quoted gap among these calculations is due to using different exchange-correlation functionals or different basis sizes. Most importantly, however, is that the previous calculations did not include spin-orbit coupling. The lowest conducting bands from Ta t_{2g} states undergo a substantial spin-orbit splitting, which reduces and inverts the gap; see Fig. 2.

[44] L. Fu, C. L. Kane, and E. J. Mele, Toplogical Insulators in Three Dimensions, Phys. Rev. Lett. **98**, 106803 (2007).

[45] See Supplemental Material at http://link.aps.org/supplemental/10.1103/PhysRevB.97.121104 for the hybrid Wannier charge center plot, band structures for breaking symmetries, and additional thermoelectric parameters.

[46] J. C. Y. Teo, L. Fu, and C. L. Kane, Surface states and topological invariants in three-dimensional topological insulators: Application to $Bi_{1-x}Sb_x$, Phys. Rev. B **78**, 045426 (2008).

[47] D. Parker and D. J. Singh, Alkaline earth lead and tin compounds Ae_2Pb, Ae_2Sn, Ae=Ca, Sr, Ba, as thermoelectric materials, Sci. Technol. Adv. Mater. **14**, 055003 (2013).

[48] G. Kresse and J. Furthmüller, Efficiency of *ab-initio* total energy calculations for metals and semiconductors using a plane-wave basis set, Comput. Mater. Sci. **6**, 15 (1996); Efficient iterative schemes for *ab initio* total-energy calculations using a plane-wave basis set, Phys. Rev. B **54**, 11169 (1996).